

A Study of External Galaxies Detected by the COBE Diffuse Infrared Background Experiment

Sten Odenwald¹, Jeffrey Newmark²,
George Smoot³

October 8, 2018

¹ Hughes STX, Code 685.9, Goddard SFC, Greenbelt, MD 20771

² Applied Research Corporation, Landover, MD 20785

³ Lawrence Berkeley Laboratory, University of California, Berkeley, CA 94720

ABSTRACT

A comparison of the COBE¹ Diffuse Infrared Background Experiment (DIRBE) all-sky survey with the locations of known galaxies in the IRAS Catalog of Extragalactic Objects and the Center for Astrophysics Catalog of Galaxies led to the detection of as many as 56 galaxies. In this paper, we present the photometric analysis of these detections and an analysis of their dust properties.

The sample is dominated by late-type spirals and active galaxies, and their far-IR continua between 25-240 μm suggest a single dust component dominating the far-IR emission. We show that for the spirals, $\langle T_d \rangle = 27.6$ K, and for the active galaxies, $\langle T_d \rangle = 35.5$ K. Estimates of the ratio of the mass of the dust component detected at $T_d = 20 - 30$ K to a hypothetical component with $T_d = 15$ K provide modest constraints to the Very Cold Dust (VCD) component present in the galaxies detected at 140 and 240 μm . VCD components with < 7 times the mass of the 20-30 K dust are consistent with all of the upper limits.

Subject Headings: Infrared:Sources, galaxies:photometry

¹ The National Aeronautics and Space Administration/Goddard Space Flight Center (NASA/GSFC) is responsible for the design, development, and operation of the *COBE*. Scientific guidance is provided by the *COBE* Science Working Group. GSFC is also responsible for the development of the analysis software and for the production of the mission data sets.

1.0 INTRODUCTION

The Infrared Astronomical Satellite (IRAS) has shown that many galaxies are strong sources of far-IR radiation, particularly at 60 and 100 μm (Soifer, Houck and Neugebauer, 1987). The nature of galactic far-IR emission among late-type spirals is widely acknowledged to be radiation reprocessed by dust grains present in a variety of sizes and temperatures in the interstellar medium (Cox and Mezger, 1989; Desert et al., 1990). This radiation may have as its origin the UV-rich light from new generations of OB stars in spiral arms; the non-thermal continuum produced by an active nuclear source (Knapp and Patten, 1991); or the diffuse interstellar radiation field itself (Mathis, Mezger and Panagia, 1983). An open question regarding the infrared properties of ‘normal’ galaxies is the number of dust components contributing to their far-IR luminosities. A perusal of the literature reveals a confusing field of possibilities identified on the basis of one or two- component black body fits to far-IR and sub-millimeter data on galaxies spanning a wide range of morphological types and levels of star-forming activity. The literature can best be summarized by defining, in an ad hoc manner, three dust components characterized by their temperature. We define Very Cold Dust (VCD) as dust having $T_d < 15$ K; Cold Dust (CD) as $15 \leq T_d < 25$ K; and Warm Dust (WD) with $T_d \geq 25$ K. The continua of galaxies often appear to be dominated by one or more of these thermal components at far-IR and sub-millimeter wavelengths.

A preliminary study of our Milky Way using the COBE, Far Infrared Absolute Spectrophotometer (FIRAS), (Wright et al. 1991) concluded that the spectral data from 121 to 2600 μm imply a two-component continuum model with a dust emission index ν^α , of $\alpha = 2.0$, and $T_{CD} = 20.4$ and $T_{VCD} = 4.77$ K. The VCD dust component, however, contributed only 0.11 % of the total dust emission. Sodroski et al. (1994) used COBE, DIRBE all-sky data to show that a pervasive CD dust component exists with $17 < T_d < 22$ K which can be detected at $60 < \lambda(\mu\text{m}) < 240$. Indeed, this component is closely associated with the diffuse HI clouds and cold molecular clouds that make up the far-IR ‘cirrus’ discovered by IRAS at 100 μm (Soifer et al., 1984).

UKIRT observations of the nuclear regions of 11 IR-bright spiral galaxies by Eales, Wynn-Williams and Duncan (1989) obtained fits to their 60 - 1100 μm continua using a single thermal component model with $\alpha = 2.0$. The dust temperatures providing the best fits were in the range from 30 - 50 K indicative of WD presumably associated with active star-forming regions. A similar IRAS/sub-mm study by Clements, Andreani and Chase (1993) of 5 bright galaxies selected from the far-IR catalog by Smith et al. (1987) also concluded that a single WD component yielded a superior fit to the photometric data with $28 \leq T_d \leq 35$. At least for luminous far-IR selected galaxies, the conclusion appears to be that a single WD dust component dominates the far-IR emission at $\lambda \geq 60 \mu\text{m}$.

Among the less active, late-type galaxies, a different population of dust grains appears to dominate the galactic emission. Chini et al. (1986) investigated a sample of 18 Sb-Sc spiral galaxies. Rather than a single WD component, they find two thermal components in the far-IR; one WD component typically has $T_d \approx 53$ K, while a cooler CD component has $T_d \approx 16$ K. Eales, Wynn-Williams and Duncan (1989) included in their study several of the galaxies observed by Chini et al. (1986) but were unable to reach the same conclusions, finding only conclusive evidence for a single CD component. The issue of one vs two thermal components

for late-type galaxies was re-opened by Chini and Kruegel (1993) in studies of NGC 660 and UGC 3490 who, again, identify two components : $T_{WD} \approx 50$ K and $T_{CD} \approx 17$ K in these galaxies. They proposed that the sub-millimeter disagreements were the result of investigators not observing galaxies with the same beam size (90"), chopper throw, and wavelength as had Chini et al. (1986).

At the present time, the controversy remains unresolved as to whether a sample of ‘normal’ spiral galaxies distinguished only by their optical rather than far-IR luminosity have one or two thermal components dominating their far-IR luminosity at $\lambda > 60 \mu\text{m}$. Thuan and Sauvage (1992) reviewed the results from a variety of often conflicting surveys, and through a series of cross-correlations between the CfA Galaxy Catalog (Huchra et al., 1992; hereafter the ‘CfA Catalog’) and the H_α survey of galaxies by Kennicutt (1983), showed that the expected correlation between star-forming activity and total far-IR luminosity does not occur in the case of ‘normal’ spiral galaxies. Star-forming regions are apparently less important in determining the integrated far-IR luminosity of a normal (non-AGN, non-starburst) spiral galaxy than some other parameter of the galaxian interstellar medium. They suggest that CD grains associated with cirrus-like dust at $T_d \approx 20$ K may be the principle source of far-IR luminosity at $\lambda > 60 \mu\text{m}$. This is consistent with the findings of Walterbos and Schwoerer (1987) and Rice et al. (1990) who showed that 85 % of the far-IR emission from M31 (Sb-type) and 40 % of the far-IR emission from M33 (Scd) are associated with cirrus-type dust. Sodroski et al. (1994) show a similar trend for the Milky Way (Sb-Sc) with the Galactic plane cirrus component contributing as much as 90 % of the far-IR luminosity.

Odenwald, Newmark and Smoot (1995; hereafter ‘Paper I’) reported the detection of 56 galaxies between 12 and 240 μm based on a comparison of the IRAS Catalog of Extragalactic Objects (Fullmer and Lonsdale, 1989; hereafter the ‘IRAS Catalog’) and the CfA Catalog, with the all-sky DIRBE survey. DIRBE’s large beam size of 0.7° makes it an ideal instrument for determining the integrated far-IR flux from an entire galaxy, not just its bright nuclear regions. With the exception of M-31 and the Magellanic Clouds, all galaxies bright enough to be detected by DIRBE will be observed as unresolvable point sources so that all photometric measurements of external galaxies are measurements of the integrated total emission. DIRBE’s photometric overlap with the IRAS 12-100 μm bands, and additional observations at 140 and 240 μm provide important constraints to the strength of any dust components with temperatures in the range from $15 < T_d(K) < 25$. Not all of the galaxies listed in Paper I were detected at 140 or 240 μm , but a significant subset of 7 galaxies were bright enough to have measurable emission at either or both of these wavelengths.

In this paper, we continue an analysis of the DIRBE galaxy sample by obtaining photometry for each galaxy in the DIRBE 12 - 240 μm bands, and refining the original detection list in Paper I. We will then use the photometric data to constrain as far as is feasible, the far-IR emitting WD, CD and VCD dust components in the detected galaxies.

2.0 OBSERVATIONS

Between December, 1989 and September, 1990, the DIRBE instrument on board NASA’s COBE satellite surveyed the entire sky in 10 photometric bands covering the wavelength region

from 1.25 to 240 μm . A detailed description of the DIRBE instrument and the COBE mission is given by Boggess et al. (1992). An extensive discussion of the absolute calibration of the DIRBE photometry may be found in the COBE, ‘DIRBE Explanatory Supplement’ (COBE,1995), but for convenience we will briefly review some of the salient issues which affect galaxy photometry.

The 2-dimensional beam profiles in the 12-100 μm bands were determined by measuring the intensity changes of numerous bright stars during the course of the entire mission as they transited the beam. For the 140 and 240 μm bands, transits of the planets Jupiter and Saturn were used. The instantaneous DIRBE beam profile in each band is constrained by an internal field stop to $0.7^\circ \times 0.7^\circ$. The beam solid angles for the 12-240 μm bands are; 1.42, 1.48, 1.51, 1.44, 1.36 and 1.33×10^{-4} sr with uncertainties of 4, 5, 15, 12, 26 and 37×10^{-7} sr respectively.

The COBE attitude control system provides information on the instantaneous pointing direction of the satellite throughout the mission. This information is provided by a combination of sun sensors, Earth horizon sensors, rate-integrating gyros and magnetometers, and is used to establish an attitude solution for each detector as a function of observing time. The rms uncertainty in the attitude solution is 0.93’ based on sightings of specific calibration objects in the near-IR 1.25 - 4.9 μm bands.

The DIRBE photometry has been corrected for detector gain variations due to environmental influences and instrument instabilities, and then calibrated to physical units. Observations of approximately 144 celestial calibrators (e.g. stars, planetary nebulae, HII regions) are then used to establish a relative photometric system which is stable over the duration of the mission. This relative photometric scale is then converted to an absolute scale by observing a small sample of well known discrete sources.

As described in the DIRBE Explanatory Supplement (§4.5.3.3) the bright star Sirius was used to calibrate the 12 μm band; the planetary nebula NGC 7027 was used for the 25 μm band; the 60 and 100 μm bands were calibrated by using the planet Uranus; and Jupiter was used for the 140 and 240 μm bands. The quadrature sum of the contributions to the absolute flux calibration in the 12-240 μm bands are (in percent): $C_F = 11.7, 15.5, 8.6, 13.7, 10.1$ and 10.1 respectively. The uncertainties in the absolute surface brightness calibration, C_I , are virtually identical. The primary source of the uncertainty is in the adopted brightnesses of Sirius, NGC 7027 and the planets Jupiter and Uranus. Also as explained in the DIRBE Explanatory Supplement (§4.5.4.2 and Table 4.5-9) a comparison of one band with the others for purposes of spectral fitting and source color determination leads to uncertainties of $\approx 15\%$ depending on the band pairs considered.

The initial detection search in Paper I was conducted using the cold mission, averaged skymap data. The positions searched for galaxy detections were obtained from the IRAS Catalog. We also searched the CfA Catalog for detections in the 4% of the sky not covered by the IRAS survey which according to the CfA Catalog included 1251 optically-identified galaxies brighter than $+14.5^m$. Initial estimates of the point source flux in the skymap data were obtained by removing a simple 2-dimensional background model from the position of each galaxy in the skymap.

In order to be considered a detection, in Paper 1 we described how the candidate had to be visible at a signal-to-noise (S/N) of at least 5.0 after background removal in a single band, or at a S/N exceeding 4 in at least two bands. In the latter case, the effective $S/N > 4\sqrt{2} = 5.6$

matched or exceeded the single-band threshold. The search was then considered to be complete to a uniform $S/N = 5$.

As the IRAS survey discovered (see Low et al., 1989), much of the sky at $\lambda > 60 \mu\text{m}$ is covered by interstellar, infrared cirrus clouds which can have considerable internal structure from a few arcminutes to many degrees in scale. Large-beam observations of such a background can lead to spurious detections of unresolved cirrus cloud features as well as bona fide non-cirrus background sources. If a candidate satisfied the S/N criterion, the surrounding $7^\circ \times 7^\circ$ field was then inspected visually to insure that the candidate could not plausibly be assigned to an unrelated cirrus feature. We also consulted the ‘‘Catalog of Infrared Observations’’ (Gezari, Schmitz and Meade, 1993) to eliminate prominent, Galactic IR sources which may coincide with the 3×3 pixel DIRBE beam patch centered on the galaxy position. The initial search (Paper I) for extragalactic detections produced 53 candidates in the IRAS Catalog, and 3 candidates in the CfA Catalog. In what follows, we will subject this initial detection list to a more rigorous analysis for spurious false detections, and obtain a final list of DIRBE extragalactic detections.

3.0 GALAXY DETECTIONS AND PHOTOMETRY

3.1 The Final Catalog

In Figure 1, we show the results of the initial search described in Paper 1. Each image represents a $7^\circ \times 7^\circ$ field centered on the pixel coinciding with the cataloged galaxy position. The ordering of the galaxies is based on the refined classification criteria we will discuss in this section. A 2nd order background model has been removed from each field, and the pixel intensities have been re-scaled, so that the intensity of the pixel nearest the galaxy position is normalized to 1.0. This particular image transformation, used only in the inspection for foreground clutter, optimizes the contrast of the foreground clutter in the field. Table 1 gives the S/N of the peak galaxy emission found in each of the DIRBE images shown in Figure 1, along with the total S/N for the candidate. For measurements near the noise limit of the sky map, some of the listed S/N s will be negative. The total S/N is computed from the square root of the quadrature sum of the individual in-band S/N s.

It is evident that many of the fields, especially those corresponding to the weakest detections such as NGC 1313 and NGC 3621, contain significant structure at 60 and $100 \mu\text{m}$. Indeed, many of the candidates with a total $S/N < 8$ show enhanced foreground clutter. The most important question we must now address is, given the large size of the DIRBE beam and the complexity of the cirrus emission, how may we insure that a particular candidate is a galaxy rather than a detection of a bright cirrus feature?

In Paper I, we utilized a simple S/N detection criterion to establish the candidate list, followed by a visual inspection of each candidate field to eliminate objects that were clearly in fields with a complex background. For example, the cometary star-forming region NGC 5367 which is a bright, compact far-IR source according to Odenwald (1988) appeared to coincide with the CfA galaxy A1356-3949. This would have resulted in a false detection of this galaxy in the DIRBE skymap data. We would now like to investigate improving the initial survey described in Paper I by utilizing a group of indices designed to characterize the presence of

cirrus emission in each field.

We present in Table 2 the revised catalog of 54 DIRBE galaxy candidates based on the results from Paper I. We do not include in this study either the Large or Small Magellanic Clouds since they were resolved by DIRBE. Excluded from this table is the nearby galaxy M-31 which DIRBE also detected as an extended infrared source. This new tabulation, moreover, does not list the previously identified DIRBE candidate ‘NGC 7625’ which was found to be the galactic source CRL 3068 located 18’ from the galaxy position. Column 1 is the galaxy name; column 2 indicates the morphological type; columns 3-4 give the Galactic latitude and longitude of the galaxy based on its IRAS or CfA Catalog positions. The degree of cirrus contamination for each galaxy field is indicated by a set of quality indices appearing in columns 5 - 12. The first four indices were obtained from the IRAS Point Source Catalog and are generally recognized as useful cirrus flags for studies of point source in the IRAS data. SES1 counts, in each band, the number of hours-confirmed small extended sources within 6’ of the identified point source. SES2 represents a similar tally for weeks-confirmed sources. According to the IRAS Explanatory Supplement (§ VII-36.H.1.b), both indices warn of the presence of extended, Galactic foreground structure. Columns 5 and 6 present the SES1 and SES2 ‘small extended source’ confusion flags at 100 μm . Values less than 2 are considered to be indicative of point sources in ‘clean’ fields. In columns 7 and 8 we present the IRAS CIRR1 and CIRR2 indices. CIRR1 gives the total number of sources detected at 100 μm in a 1 square degree box centered on the IRAS point source. Values exceeding 3 indicate significant cirrus or extended emission. CIRR2 is the logarithmic ratio of the point source 100 μm flux to the cirrus flux from spatially-filtered 0.5° IRAS data. Values exceeding 3 also indicate significant cirrus contamination. The CIRR1 and 2 indices are well-matched to the DIRBE beam and will be given higher weight than the comparatively small angular scale ($\approx 6'$) SES1 and SES2 indices.

One of the difficulties in using the IRAS cirrus flags as a final arbiter of whether or not the candidate is a cirrus feature is that objects such as M33, M82 and even NGC253 have large CIRR1 indices. In a fully automated search for detections, these galaxies would be overlooked in favor of other fainter candidates such as NGC 4102 or NGC 4038 which have lower cirrus indices. This suggests that the IRAS-based SES and CIRR indices cannot constitute the entire basis for deciding between a detection of clutter and the detection of a galaxy in the DIRBE skymap data. We have, therefore, defined three new indices appropriate for DIRBE skymap data which provide a measure of the underlying structure of the foreground against which each galaxy is seen. N3x3, presented in column 9 of Table 2, represents the number of IRAS point sources found in the 3×3 pixel beam patch centered on the galaxy. This index is similar to the IRAS CIRR1 index, but includes all IRAS point sources, not just those detected only at 100 μm . For IRAS-detected galaxies its minimum value is unity. Values larger than this can occur if the galaxy is resolved by IRAS, or if the IRAS field contains a number of bright, discrete features in the infrared foreground. We define a second index, N100, as the number of 100 μm IRAS sources (excluding the candidate galaxy) that were counted in N3x3, and which are brighter than 10 % of the galaxy’s peak IRAS flux appearing in the IRAS Point Source Catalog. The final index, RB, is the ratio of the rms background 100 μm intensity of the DIRBE skymap region within 2° of the galaxy (but not including the 3x3-pixel galaxy patch), and the rms of a sky patch within 2° of the North Galactic Pole. After the removal of a smooth background gradient, the NGP

region was found to have an rms intensity of 0.72 MJy/sr at 100 μm . Values for RB near unity indicate that the galaxy is situated in a region with essentially the same degree of detectable clutter at a scale of a few degrees as compared with the reference region near the North Galactic Pole. Values near RB = 0 indicate that the galaxy region has less clutter than even the North Galactic Pole. In column 12, we also present the total S/N for the galaxy candidate obtained from a quadrature sum of the individual S/Ns for each of the 6 bands we surveyed.

Comparing the various confusion flags in Table 2 against the fields in Figure 1, we see no simple correlation between detectability and background clutter without exempting a number of galaxies from the analysis. The CIRR1 and CIRR2 indices yield more clutter discrimination at the scale of the DIRBE beam and show that in addition to M82 and M101, the galaxies M33, NGC 1313, NGC 3256 and NGC 4945 have values exceeding 3. These are, therefore, suspect of having cirrus contamination and would have to be eliminated as detections in a conservative cataloging of DIRBE galaxy candidates.

The collection of indices, N3x3, N100, RB, SNR, derived from the DIRBE and IRAS data yield a better measure of the amount of clutter in each field, in particular, the RB and total S/N indices. From a comparison of Figure 1 with the RB index in Table 2, column 11, and the total S/N for the candidate in column 12, we propose the following algorithm for reducing false detections due to cirrus or other foreground clutter in our sample.

All candidates with $S/N > 15$ will be considered positive detections. This yields a sample of 17 galaxies which we identify as Group A. With the exception of M82, NGC 4945, NGC 5128 and IC 342, the Group A galaxies have $RB \leq 3$ and $CIRR2 \leq 3$, both indicating minimal background cirrus clutter in the immediate vicinity of each galaxy. The large RB value for M82 is the result of the presence of a bright cirrus feature near M82 which is apparent in Figure 1. The galaxies NGC 1808 and IC 342, on the other hand, have the most cluttered fields of the galaxies in this group. Their index sets (SES1, SES2, CIRR1, CIRR2, RB) are (0,0,1,1,2) and (4,1,0,3,15) respectively, and indicate that only IC 342 has a significant probability of being a false detection of cirrus.

We define Group B candidates as detections which have $8 < S/N < 15$, and as for Group A, $RB \leq 3$. This sample of 17 galaxies has $SES2$ and $CIRR2 \leq 2$ indicating relatively low cirrus contamination. At the scale of the DIRBE beam, and over a region of 7° , Figure 1 shows that unlike Group A, and despite their low cirrus indices in Table 2, some of the fields, nevertheless, contain some clutter, particularly NGC 4490 and NGC 613.

The third, Group C, represent the fainter candidates in this survey and have $5 < S/N < 8$. Of these, NGC 891, NGC 1097A, NGC 3256, NGC 3621, NGC 5128 and IC 751, are adjacent to bright regions of cirrus emission and unlike M82, have insufficient S/N to readily distinguish them from bright cores in the cirrus emission other than by virtue of their coincidence with the galaxy positions. NGC 891, NGC 1097A and NGC 5128, nevertheless, represent the more plausible galaxy detections among these 6 candidates.

From the previous analysis, we conclude that the 39 members of Group A and B constitute the most reliable extragalactic detections obtained from the DIRBE skymap data at 12-240 μm .

3.2 Point Source Photometry

The DIRBE skymaps have been optimized for preserving the photometric accuracy of extended emission at scales larger than the DIRBE beam. The time-ordered data is the preferred data to use to obtain accurate point source photometry, however, this is a time consuming procedure beyond the scope of the present study. Point source photometry used in this study is derived from the cold, mission-averaged DIRBE skymap data. A correction factor is applied to the peak emission detected towards a galaxy to reflect the true beam response.

Due to the pixelization procedure, the peak IR emission from a galaxy or other unresolved source identified in the skymap data may be up to $\pm 1/2$ pixel from its nominal optical position. Moreover, since the DIRBE beam response function is not flat over its full field of view, this can cause the galaxy emission peak detected by DIRBE to be as much as 1 pixel different from the true galaxy position. We have compensated for these effects by calculating the response of the DIRBE beam in each band at the location of the galaxy rather than at the skymap position by using an azimuthally - averaged template of the beam response computed from many transits of calibrator sources across the beam (Odegard, 1995). From the beam template at the position of the optical galaxy, we determined the responsivity of the detector, R_b , and then used the skymap flux density at this pixel, S_p , to obtain a corrected peak flux density, $S_c = S_p/R_b$. Typically, $0.9 < R_b < 1.0$ so the correction was, generally, less than 10%.

The results of this photometric analysis are presented in Table 3. Column 1 is the galaxy name; column 2 is the galaxy type; column 3 is the maximum B-band angular size in arcminutes of the optical galaxy based on the tabulations of D_{25} by de Vaucouleurs et al. (1976, 1991); columns 4-9 give the background-subtracted and beam response corrected DIRBE peak flux densities, S_c , in Janskys or their $3\text{-}\sigma$ upper limits. A color correction must be applied to the photometric values in Table 3 if the source effective temperatures are different from that of the DIRBE absolute calibrators. Tables of these correction factors may be found in the DIRBE Explanatory Supplement (e.g. Appendix B). As we can see in column 3, the maximum angular sizes of the galaxies are, with few exceptions, smaller than the $42'$ DIRBE beam. For the purposes of galaxy photometry, this large beam size implies that all but the nearest galaxies (e.g. M-31, the LMC and the SMC) will remain unresolved.

4.0 CONTINUUM FITTING

We assume that the dust emissivity follows the canonical ν^α law with $\alpha = 2.0$ (see Eales et al., 1989; Wright et al., 1991). For a galaxy for which photometry exists in two or more bands, the photometry can be fit to obtain estimators for the dust temperature, T_d , and the optical depth, τ_{100} , at $100 \mu\text{m}$ by using a dust emission function of the form:

$$I(\nu) = \tau_{100}(\nu/\nu_{100})^{2.0}B(\nu, T_d)$$

where $B(\nu, T_d)$ is the Planck function evaluated at a temperature T_d and a frequency ν . Color corrections have been applied to the DIRBE photometric data since according to the COBE Explanatory Supplement (1995), these corrections (C), defined as $I_{true} = I_{observed}/C$, are significantly different from unity between $12 - 240 \mu\text{m}$. The color corrections were determined as follows: The spectral fits were first determined without the corrections. A mean color correction was then applied representative of the average fitted temperature. For a dust grain index of α

= 2.0, the mean temperature of the entire galaxy sample was found to be $\langle T_d \rangle = 30.2$ K. The dust model fits were then recomputed for the color-corrected DIRBE fluxes to obtain the final fitted dust temperatures and optical depths for each galaxy. The use of color-corrected DIRBE fluxes leads to no significant change in the resulting fitted dust temperatures, but does produce an $\approx 20\%$ increase in τ_{100} compared to the uncorrected dust model fits, which is significant when estimating galactic dust masses. The result of this single-component dust fitting is presented in Table 4. Columns 1 and 2 are the galaxy name and morphological class; columns 3 and 4 give the fitted temperature and its uncertainty.

The galaxies in Table 4 have been segregated according to their morphological types so that any trends in the dust temperatures could be more easily recognized. The preponderance of the galaxies are late-type spirals, and systems identified as ‘active’ or ‘peculiar’ either as Seyferts, LINERS, or tidally - interacting. Based on the fitted temperatures and their uncertainties, we can derive a weighted, mean temperature for each class defined as, $\langle T \rangle_w = \Sigma(T_i/\sigma_i^2)/\Sigma(1/\sigma_i^2)$ with $\langle \sigma \rangle_w^2 = 1/\Sigma(1/\sigma_i^2)$ (see Bevington, 1969). The weights, σ_i , were determined from the individual black body fits to each galaxy’s photometric data.

The mean, weighted dust temperatures span a range from 27 - 35 K, with specific class temperatures of 27.6 ± 0.1 K for the spirals, 26.7 ± 0.3 K for the barred spirals, and 35.5 ± 0.1 K for the active galaxies. The uncertainties are biased in favor of the small number of galaxies in each cohort which have the lowest temperature uncertainties. The spirals and barred spirals do not differ significantly from one another, however, the active galaxies are significantly warmer.

The galaxies form two groups in which a WD component is dominant for the AGN and starburst-type systems, and where a CD component appears to be dominant in the remaining non-AGN/starburst galaxies. This is, of itself, not a new result, but is corroborative of findings by other investigators when similar categories of galaxies are compared.

4.1 Dust Masses

Using the single thermal component fits as an initial model, we can investigate whether significant VCD may also be present in these galaxies based on the upper limits or detections at 140 and 240 μm . Black body dust grains with $T_d = 15\text{K}$ have their peak emission at 245 μm and contribute only 25 % of their peak emission at 100 μm , which means that the DIRBE 240 μm band is optimally placed to measure the strength of this thermal component. Assigning a temperature of 15 K to this VCD component, and subtracting the fitted, one-component thermal model from the measured continuum, we can estimate from the residual 240 μm emission or its upper limit, a mass limit for this VCD that would be consistent with the galaxy continua as measured by DIRBE.

For dust grains with an emissivity coefficient, $Q_\nu \propto \nu^1$, the dust mass based on the galaxy’s measured infrared flux density, the estimated dust temperature, and its distance is given by Knapp (1991) and Clements, Andreani and Chase (1993) as,

$$M_d = 4.8 S_{100} D^2 (\exp(144/T) - 1)$$

where S_{100} is the residual flux density, or its upper limit, at 100 μm in units of Janskys, D is the distance to the galaxy in megaparsecs, and T is the assumed dust temperature. This can

be rescaled for dust grains with $Q_\nu \propto \nu^2$ as,

$$M100 = 3.4S_{100}D^2(\exp(144/T) - 1)$$

For purposes of estimating the mass of the emitting cirrus-like dust in each galaxy, which we define as M100, we use the temperature for the far-IR emission obtained from our single-component spectral fits. Table 4 presents the derived dust properties obtained in this way for the galaxies in Table 3 with known distances. In column 3 and 4 the fitted temperature and its uncertainty are given; column 5 is the adopted distance to each galaxy obtained from the listings by Huchtmeier and Richter (1989), and the redshifts tabulated by Spinoglio and Malkan (1989) with $H_0 = 75 \text{ km sec}^{-1} \text{ Mpc}^{-1}$; and column 6 is the estimated mass of the fitted dust component.

We also provide upper limits to the mass of a potential VCD component in each galaxy with an adopted temperature of 15K by computing the difference between the DIRBE photometry at $240 \mu\text{m}$, and the predicted level of the fitted thermal component detected at shorter wavelengths. The relevant relation between the far-IR emission limit at $240 \mu\text{m}$ and the effective dust mass, M240, is given by,

$$M240 = 270S_{240}D^2(\exp(59/15) - 1)$$

The resulting upper limits are presented in Table 4, column 7, together with the distance-independent ratio of M240/M100 in Column 8.

We see that the DIRBE observations provide modest constraints on the magnitude of a hypothetical 15 K VCD component in M33, M63, M83, NGC 253 and NGC 4945 on the basis of direct detection of the far-IR continuum level for these galaxies at 140 and/or $240 \mu\text{m}$. This component may not be larger in total emitting mass than about 5 - 7 times the detected CD component at $100 \mu\text{m}$ for M63 and M33, and not more than about 30 times the detected CD components in NGC 253, NGC 4945 and M 83. These galaxies appear to be well-fit by a single thermal component at $\lambda > 100 \mu\text{m}$. This strongly suggests that there are not large quantities of dust within these galaxies that are coupled together by a large-scale thermal gradient between 30 K - 15 K. This is analogous to what is observed in the Milky Way in which the dominant component is the 17 - 22 K cirrus dust emission, with no other significant reservoir of dust detectable by the COBE FIRAS experiment in the range from 17 - 10 K. We note, however, that VCD near 5 K could be present with significantly more mass in the detected galaxies than indicated by our upper limits for the hypothetical 15 K component, and still remain undetectable by DIRBE at $240 \mu\text{m}$.

For the remaining galaxies not detected at $240 \mu\text{m}$, the limits are considerably less restrictive and in many cases can accommodate as much as 100 times as much dust by mass at temperatures near 15 K as at 20 - 30 K. Sub-millimeter observations of these galaxies are clearly required to improve these restrictions to astrophysically interesting levels.

5.0 SUMMARY

From an initial catalog of 56 candidates, we present refined catalogs of galaxies detected

by DIRBE. The sample is dominated by spiral-type galaxies with effective dust temperatures similar to Galactic cirrus emission. This shows that dust similar to Galactic cirrus is at least thermally a common ingredient of late-type galaxies such as the Milky Way.

An investigation of the continua of these galaxies show them to be consistent with a single WD-like dust component which has its peak emission near $100 \mu\text{m}$, with temperatures from 25 - 35 K. Galaxies identified as active or morphologically peculiar are systematically warmer than the late-type spirals which dominate this sample. A comparison of the mass ratios of a possible 15K dust component to the warmer 20-25 K dust in the DIRBE-detected galaxies indicates that 15 K dust can exist in many of these galaxies in quite large amounts compared with the detectable cirrus-like components seen in our own Milky Way by DIRBE and IRAS.

ACKNOWLEDGMENTS

The authors gratefully acknowledge the efforts of the DIRBE data processing and validation teams in producing the high-quality datasets used in this investigation. COBE is supported by NASA's Astrophysics Division. Goddard Space Flight Center, under the scientific guidance of the COBE Science Working Group, is responsible for the development and operation of COBE.

Figure Captions

Figure 1

This figure presents the sky regions surrounding each of the DIRBE galaxies identified in Table 1. The field of view in each band is 21×21 pixels at a resolution of $21''/\text{pixel}$. The images in each band have been logarithmically stretched to facilitate the characterization of the degree of background clutter. The galaxies are grouped following their entries in Table 1 in which the S/Ns for the galaxy in each band is also presented.

Figure 2

The fitted spectra of the galaxies described in Table 4. Upper limits for the DIRBE photometry are defined as 3 times the residual background emission following the removal of a planar background model. The photometric uncertainties for the measured flux densities are the 1-sigma total photometric error defined as the rms quadrature sum of the absolute photometric uncertainty and the background fitting uncertainty. The dashed and solid curves show the continua produced from dust models involving emissivity laws of $\nu^{2.0}$ and $\nu^{1.5}$ respectively.

References

- Bevington, P. R. 1969, "Data Reduction and Error Analysis for the Physical Sciences", (McGraw-Hill Book Co.), p.130.
- Boggess, N. et al. 1982, ApJ 397, 420.
- Chini, R. et al. 1986, AA 166, L8.
- Chini, R. & Krugel, E. 1993, AA 279, 385.
- Clements, D.L., Andreani, P. & Chase, S.T. 1993, MNRAS 261, 299.
- COBE Diffuse Infrared Background Experiment (DIRBE) Explanatory Supplement, eds. M.G. Hauser, T. Kelsall, D. Leisawitz, and J. Weiland, COBE Ref. Pub. No. 95-A (Greenbelt, MD:NASA/GSFC).
- Cox, P. & Mezger, P.G. 1989, Astro. & Astrop. Rev. 1, 49.
- Desert, F.-X., Boulanger, F. & Puget, J.L. 1990, AA 237, 215.
- Eales, S.A., Wynn-Williams, C.G. & Duncan, W.D. 1989, ApJ 339, 859.
- Fullmer, L. & Lonsdale, C. 1989, NSSDC Archive Number 7113.
- Gezari, D.Y., Schmitz, M., Pitts, P.S. & Mead, J.M. 1993, "Catalog of Infrared Observations", NASA Reference Publication 1294
- Hildebrand, R. et al. 1985, Icarus, 64, 64.
- Huchra, J.P. et al. 1992, NSSDC Archive Number 7144.
- Huchtmeier, W.K. & Richter, O.G. 1989, "A General Catalog of HI Observations of Galaxies", (Springer-Verlag, NY).
- IPAC Users Guide, Edition 4, 1989, prepared by L. Fullmer et al., (JPL, Pasadena).
- Kennicutt, R.C. 1983, ApJ 272, 54.
- Knapp, G.R. & Patten, B.M. 1991, AJ 101, 1609.
- Low, F. et al, 1989, ApJ (Letter) 278, L19.
- Mathis, J. Mezger, P. & Panagia, N. 1983, AA 128, 212.
- Odegard, N. 1995, Private Communication.
- Odenwald, S., 1988, ApJ 325, 320.
- Odenwald, S., Newmark, Jeffery, & Smoot, George, 1995, IAU Symposium 168; April 24-26, 1995, University of Maryland.
- Rice, W. et al. 1990, ApJ 358, 418.
- Smith, B.J. et al. 1987, ApJ 318, 161.
- Sodroski, T. et al. 1994, ApJ 428, 638.
- Soifer, B.T. et al. 1989, AJ 98, 766.
- Spinoglio, L. & Malkan, M.A. 1989, ApJ 342, 83.
- Thuan, T.X. & Sauvage, M. 1992, in "Physics of Nearby Galaxies: Nature of Nurture?", eds. T.X. Thuan, C. Balkowski and J.T.T. Van, (Editions Frontieres: Gif-sur-Yvette Cedex, France), p. 111.
- Walterbos, R.A.M. & Schwering, P.B.W. 1987, AA 180, 27.
- Wright, N.L. et al. 1991, ApJ 381, 200.

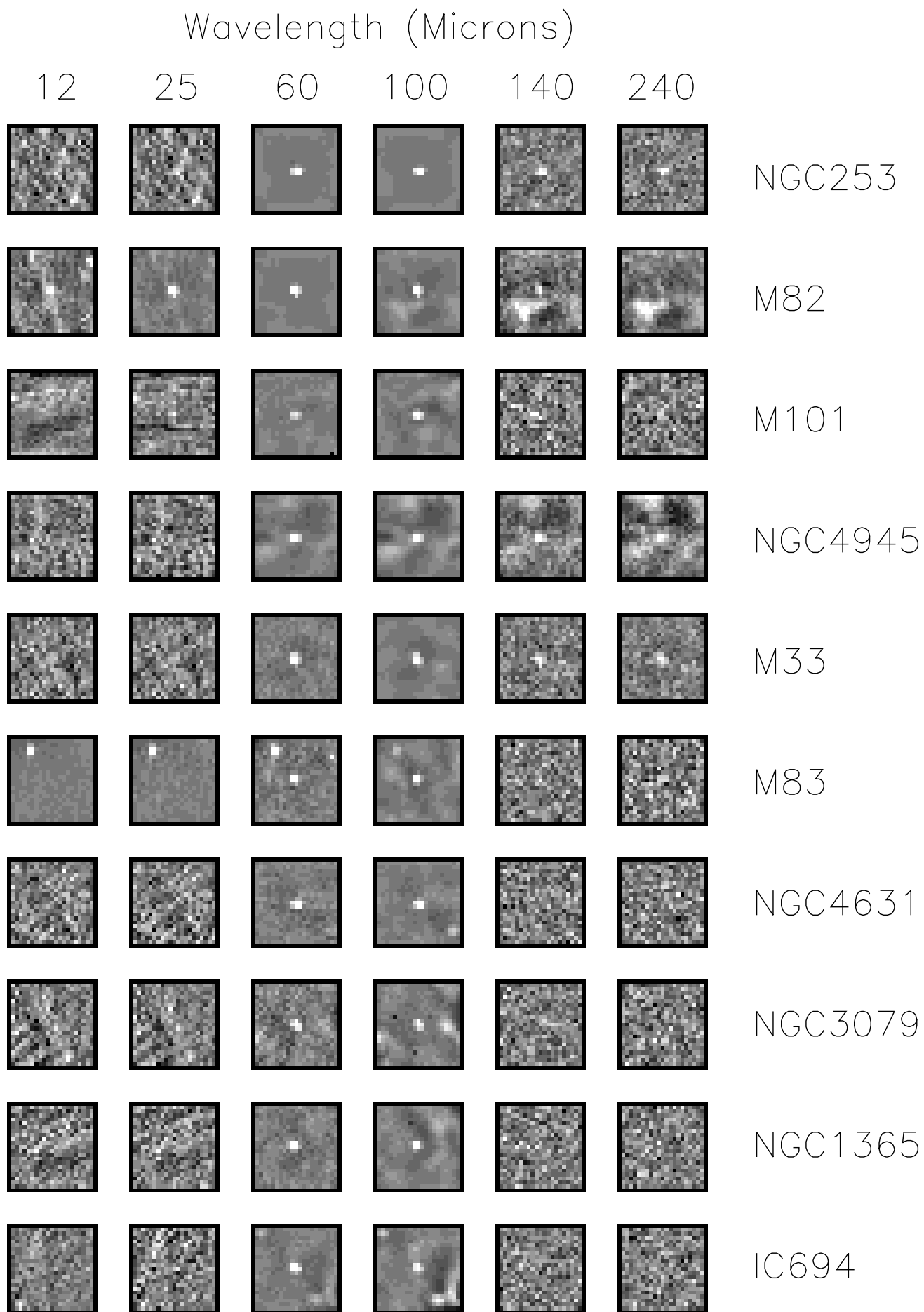


Figure 1(a)

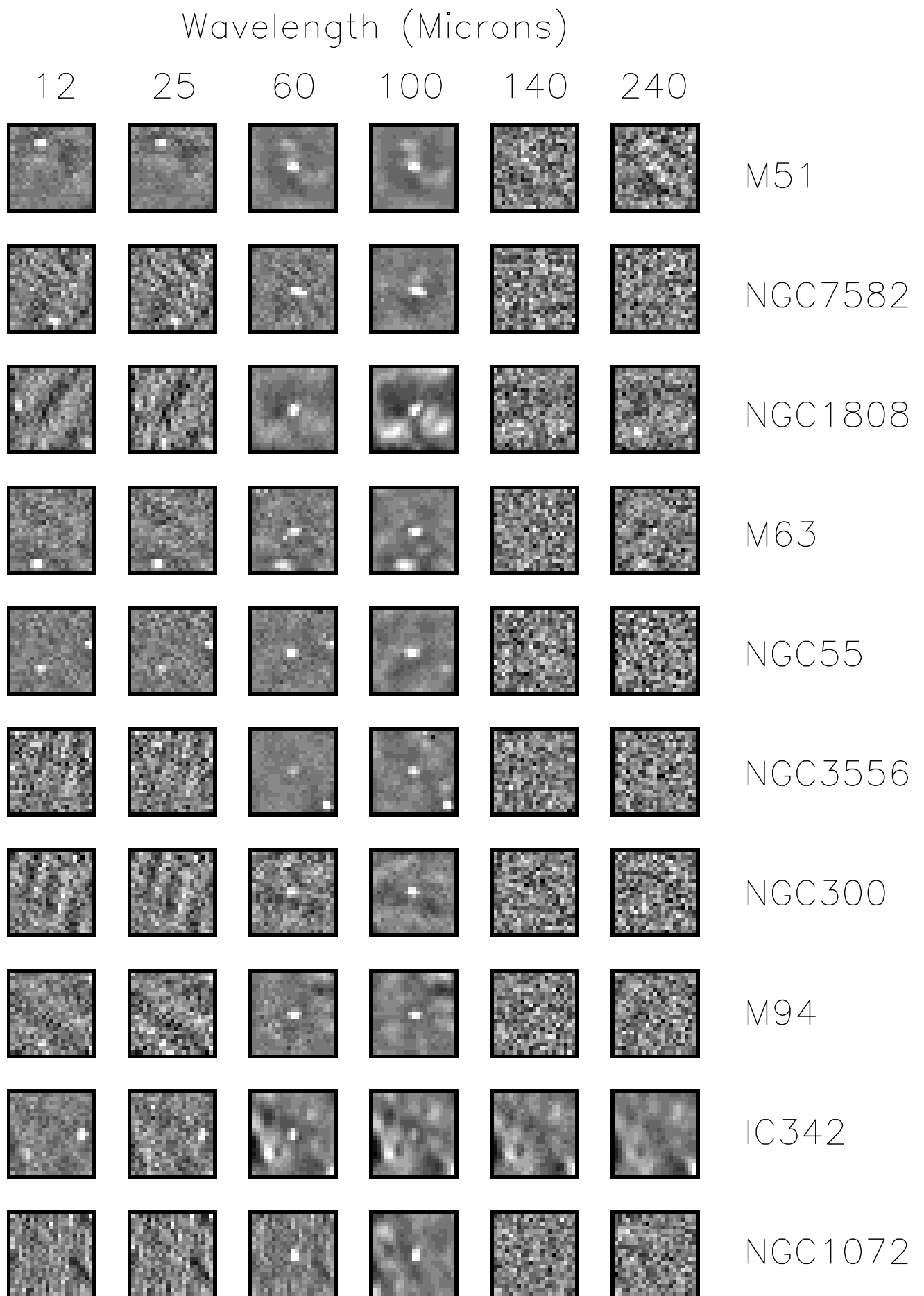


Figure 1(b)

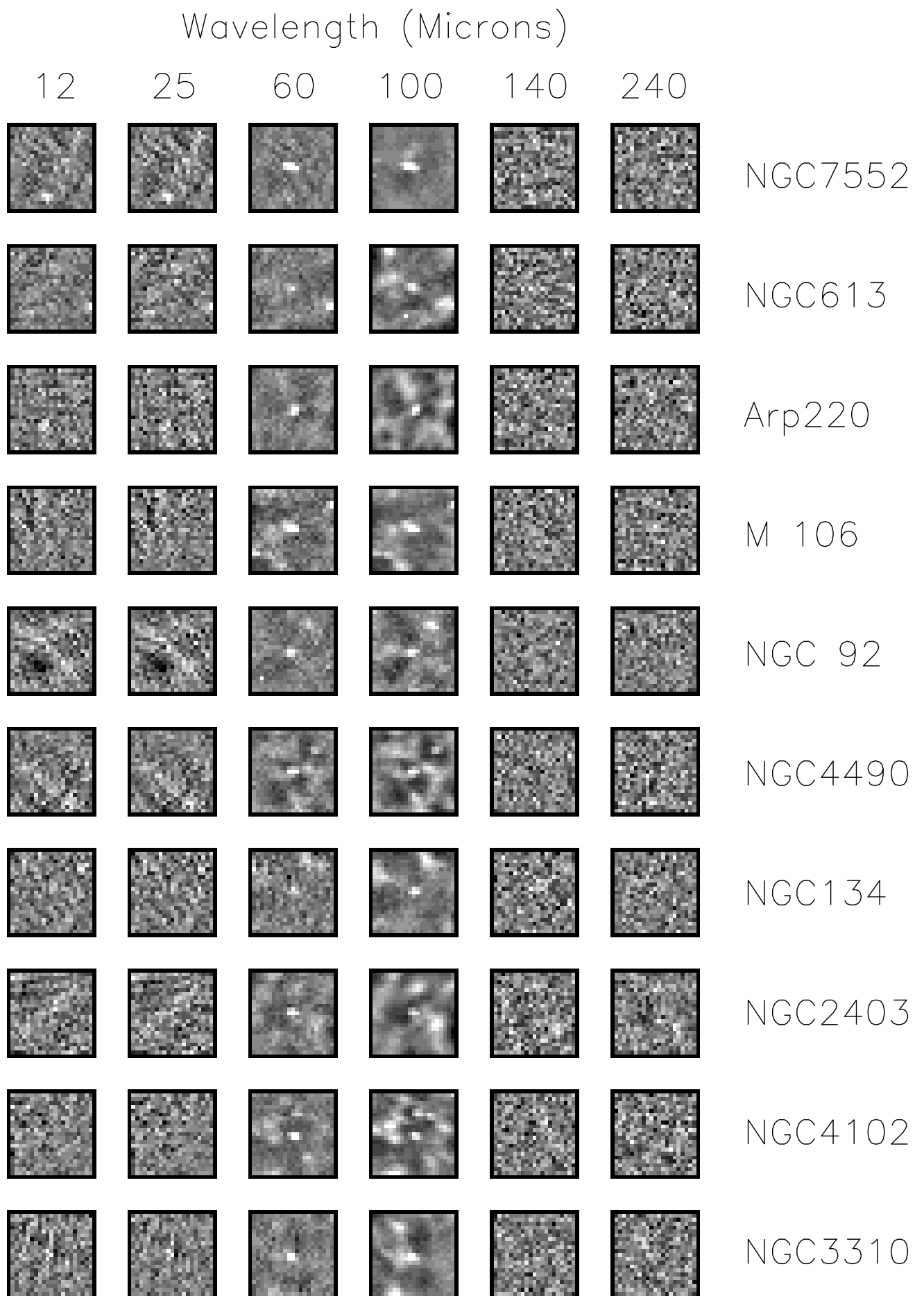


Figure 1(c)

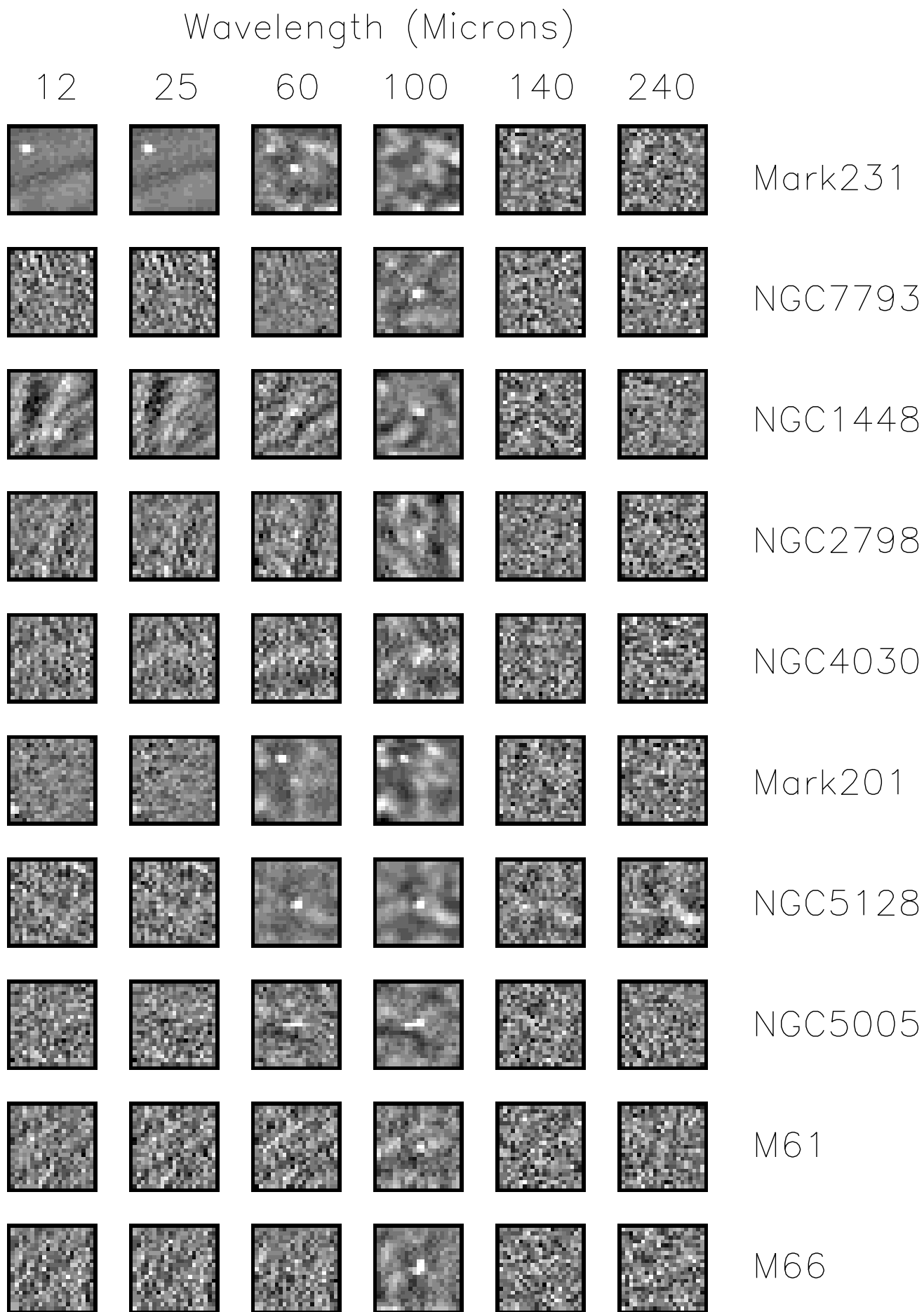


Figure 1(d)

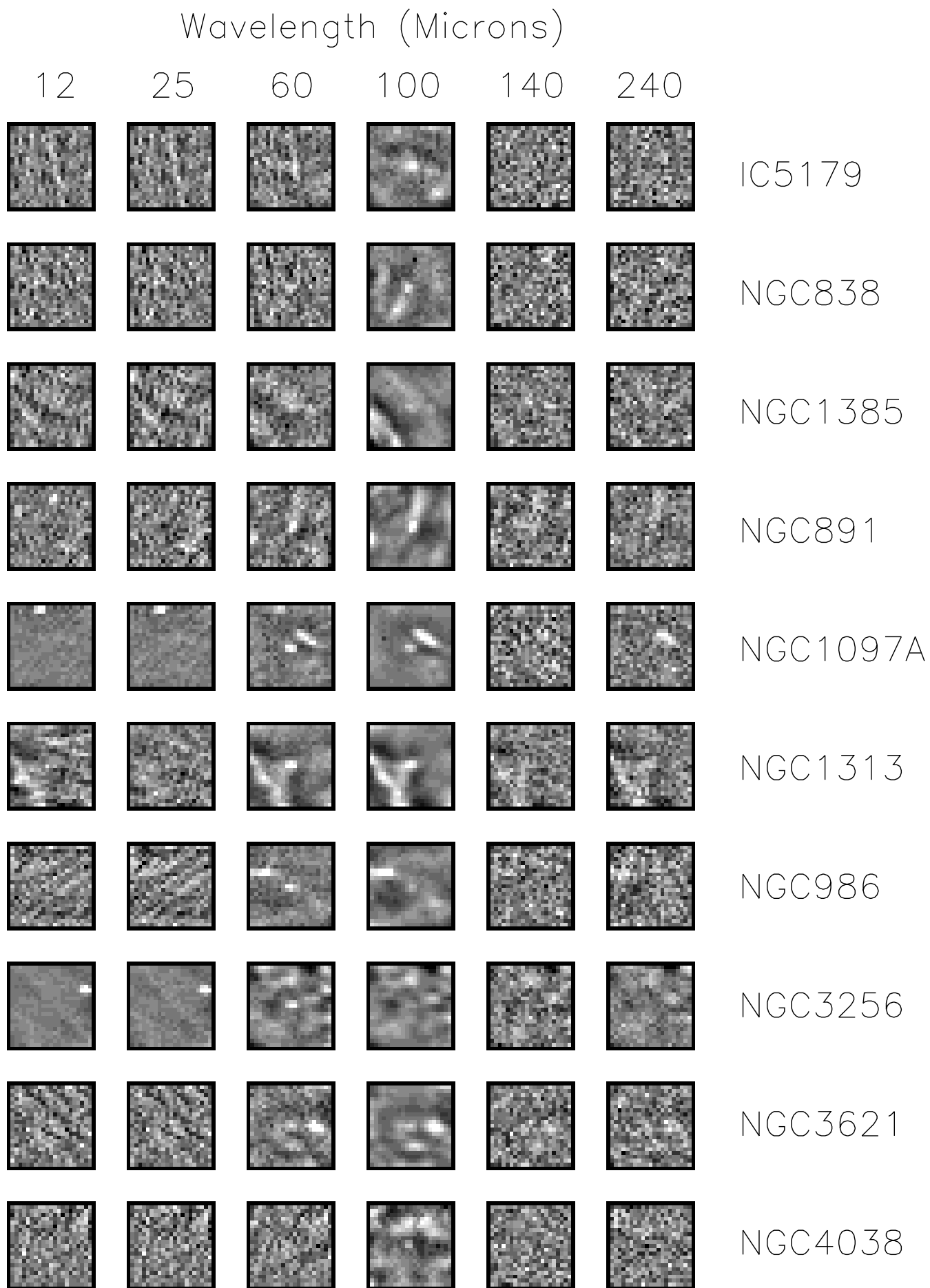


Figure 1(e)

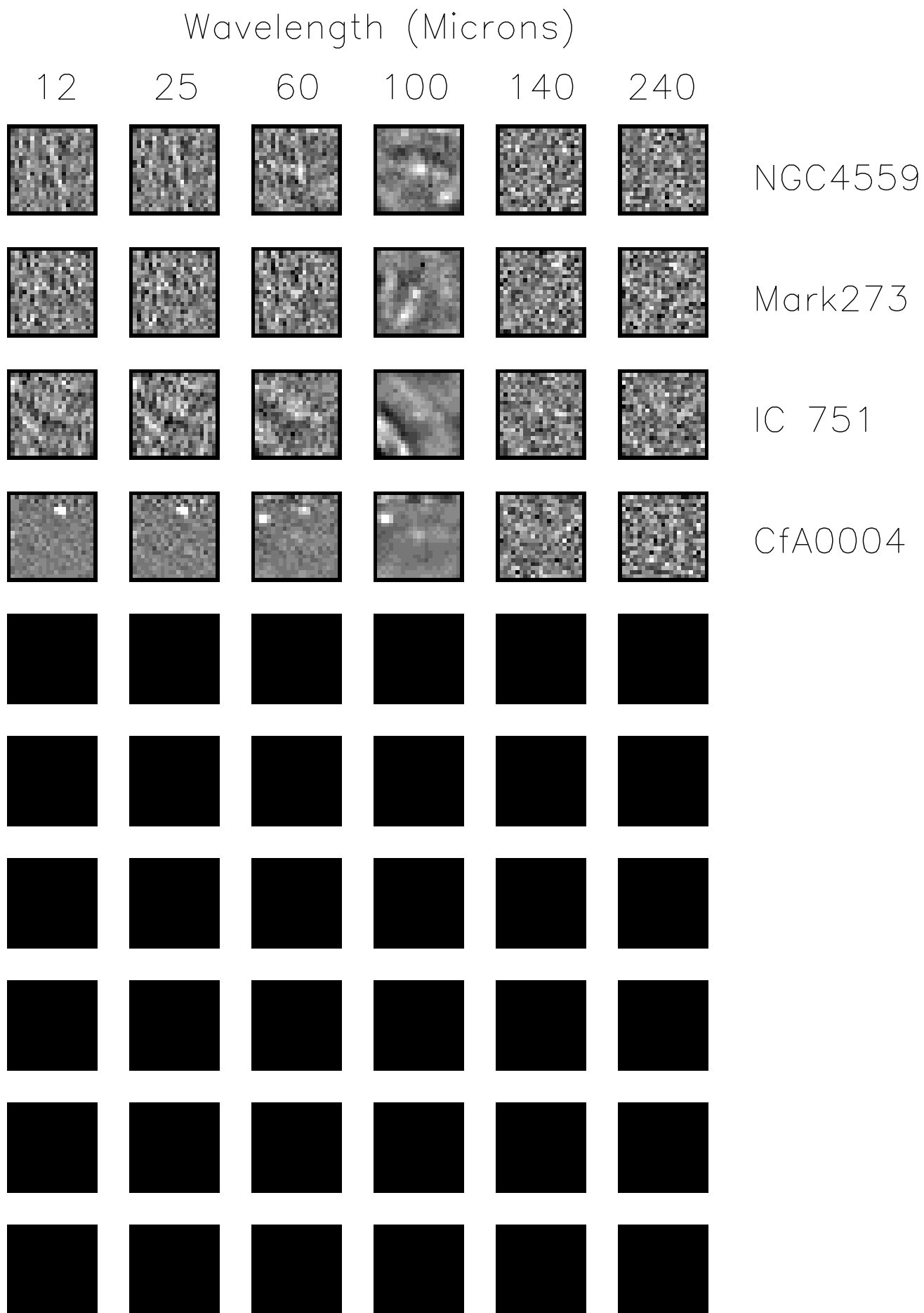


Figure 1(f)

Figure 2(a)

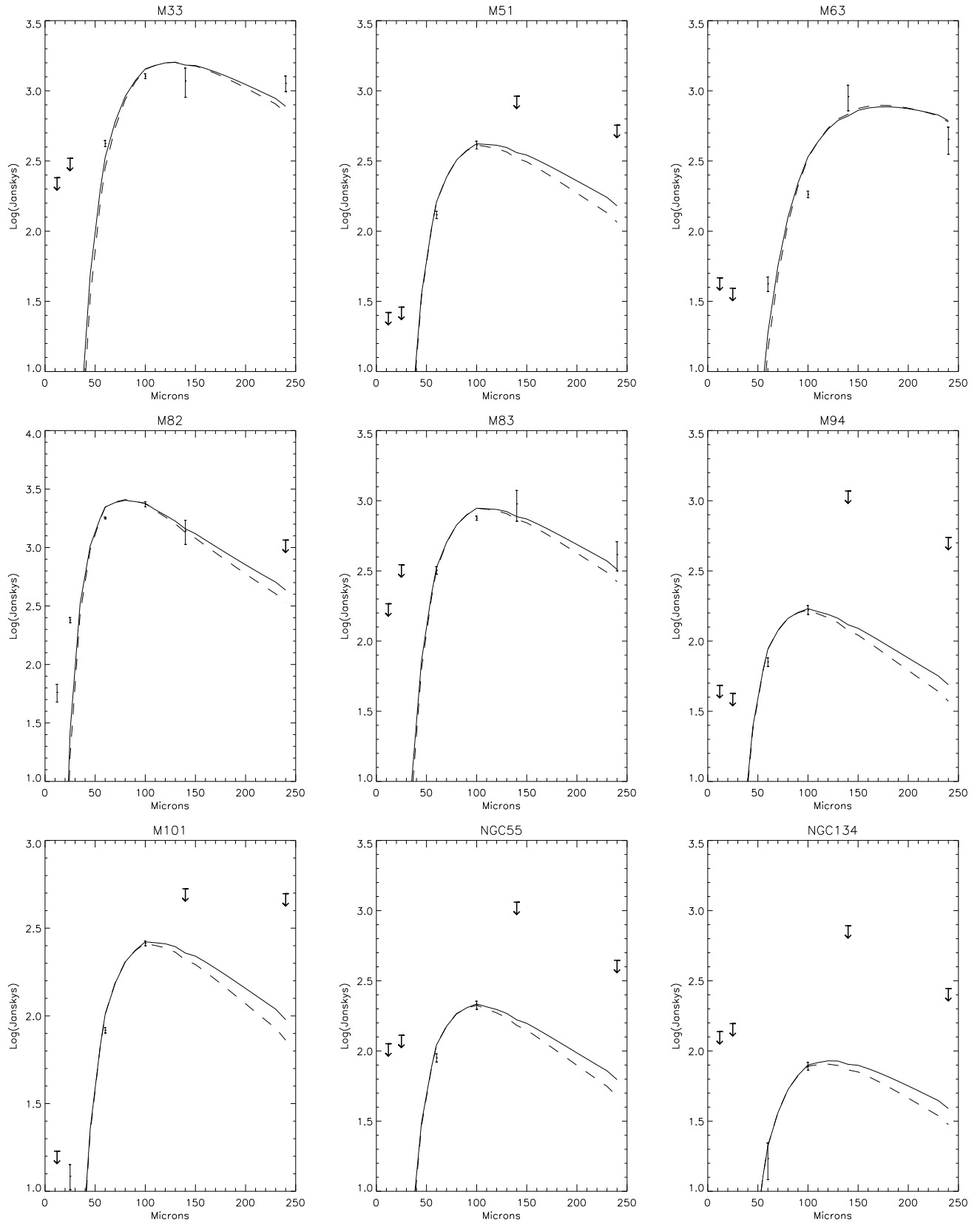


Figure 2(b)

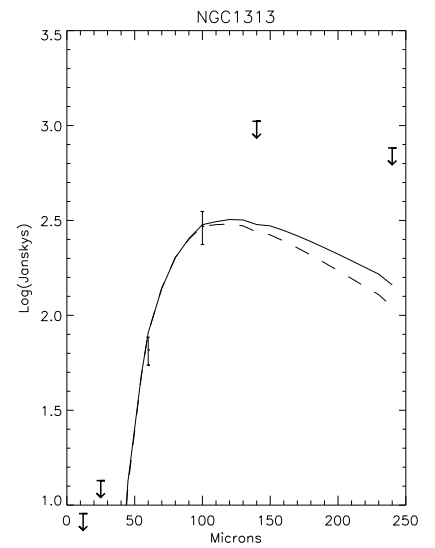
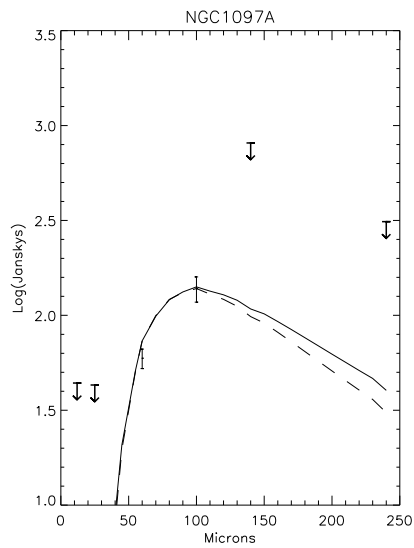
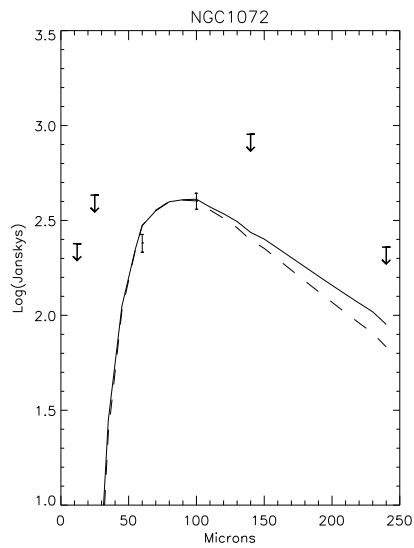
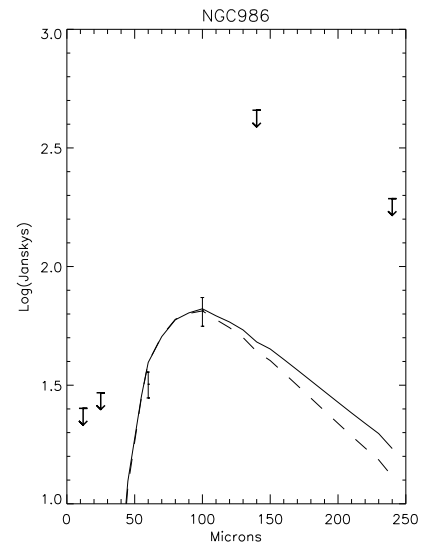
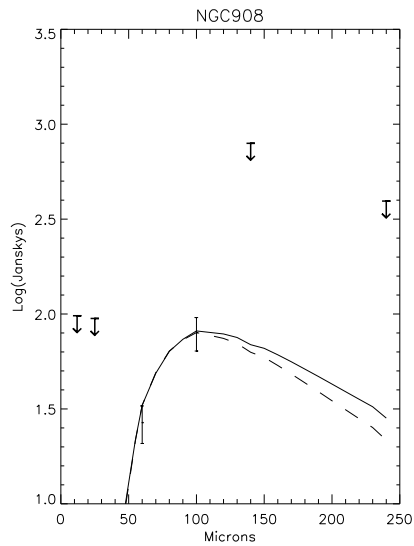
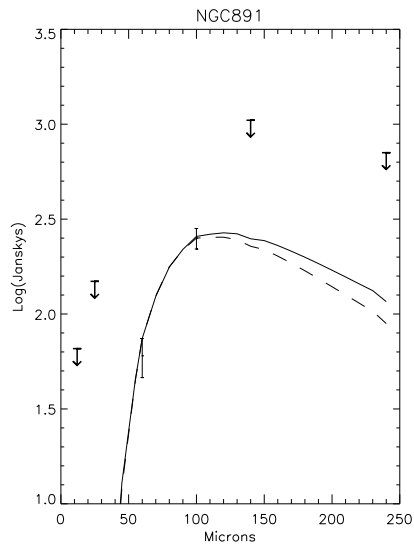
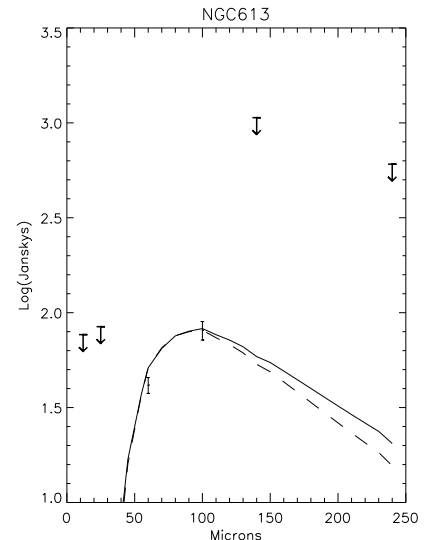
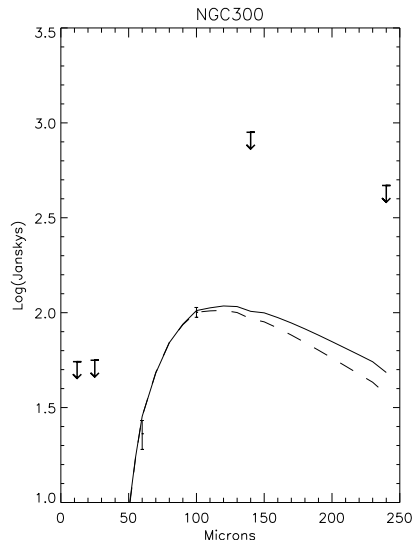
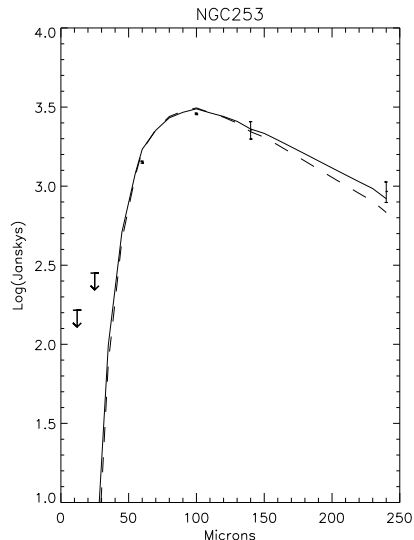


Figure 2(c)

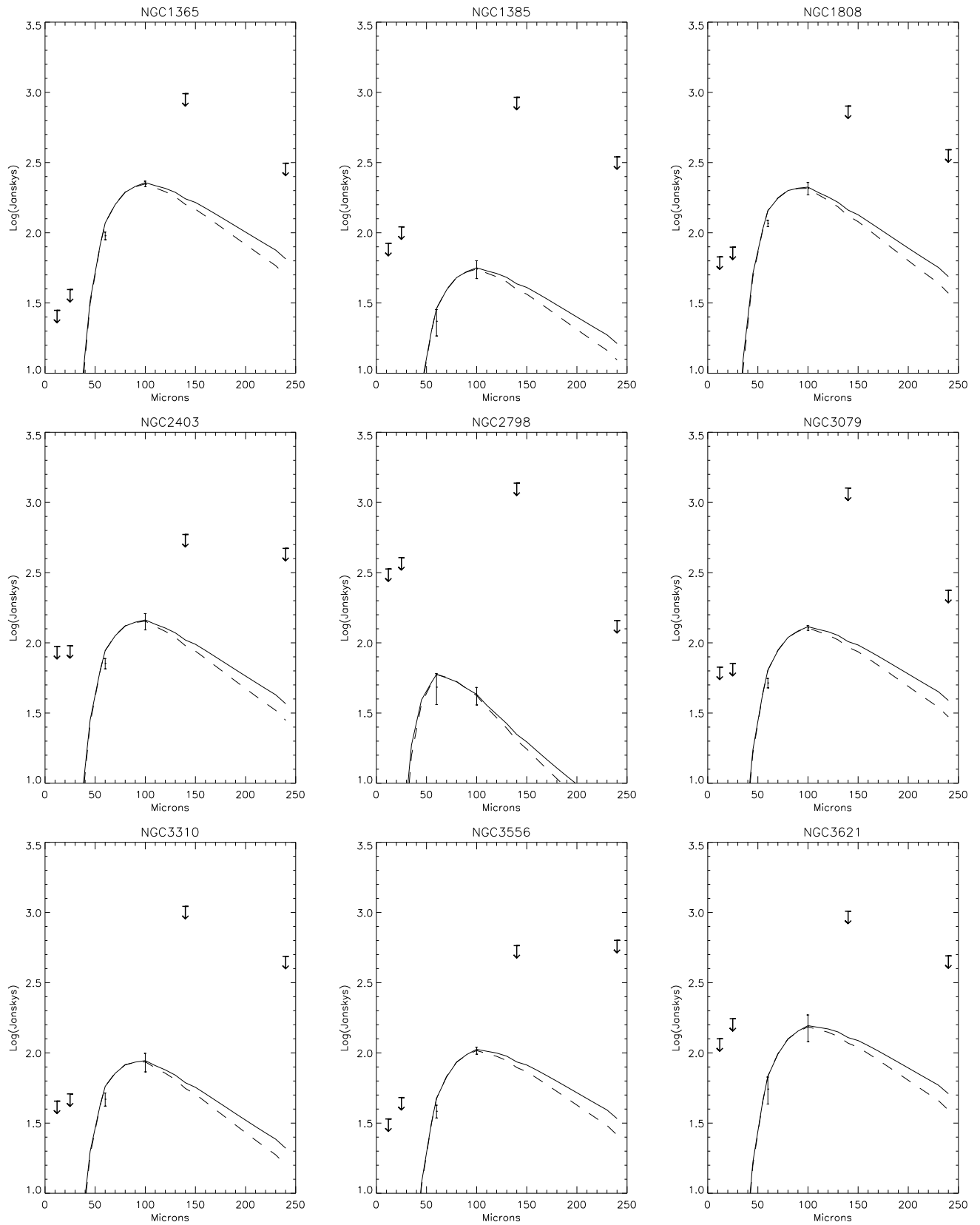


Figure 2(d)

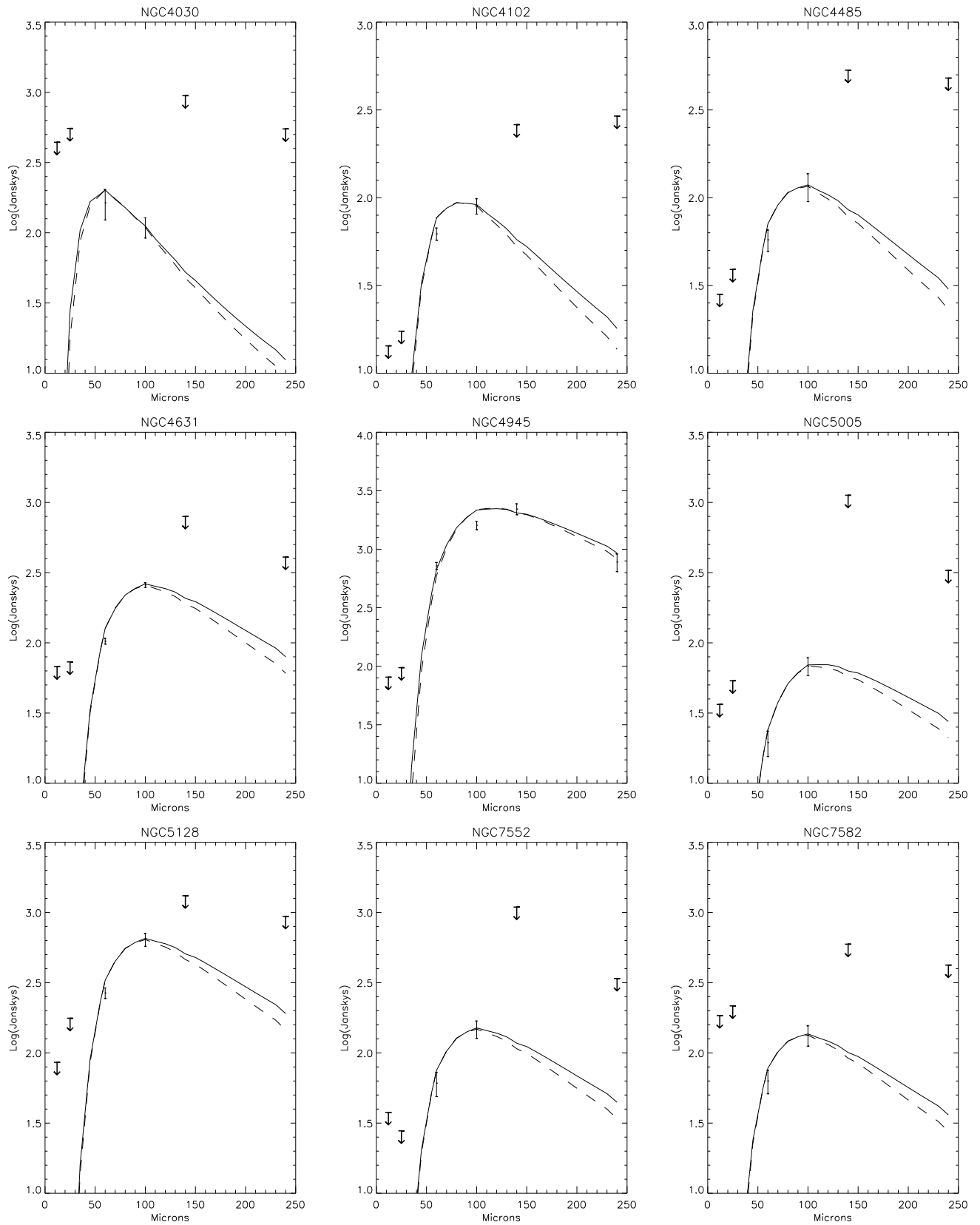


Figure 2(e)

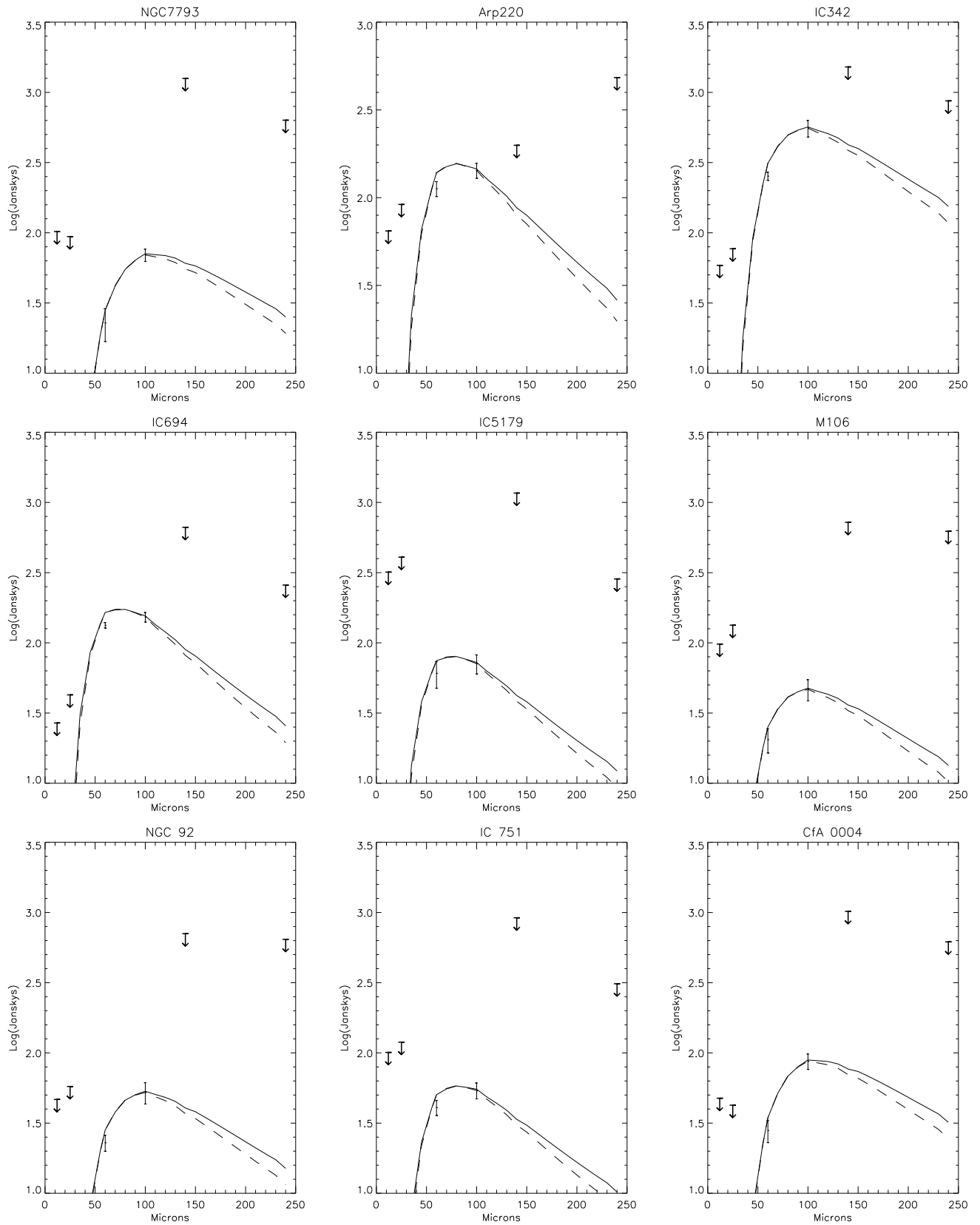


Figure 2(f)

Figure 2(g)